Electronic Supplementary Material (ESI) for Molecular BioSystems.

Systems biosynthesis of secondary metabolic pathways within the oral human microbiome member *Streptococcus mutans*

Rostyslav Zvanych, Nikola Lukenda, Xiang Li, Janice J. Kim, Satheeisha Tharmarajah and Nathan A. Magarvey

Supplementary Information:

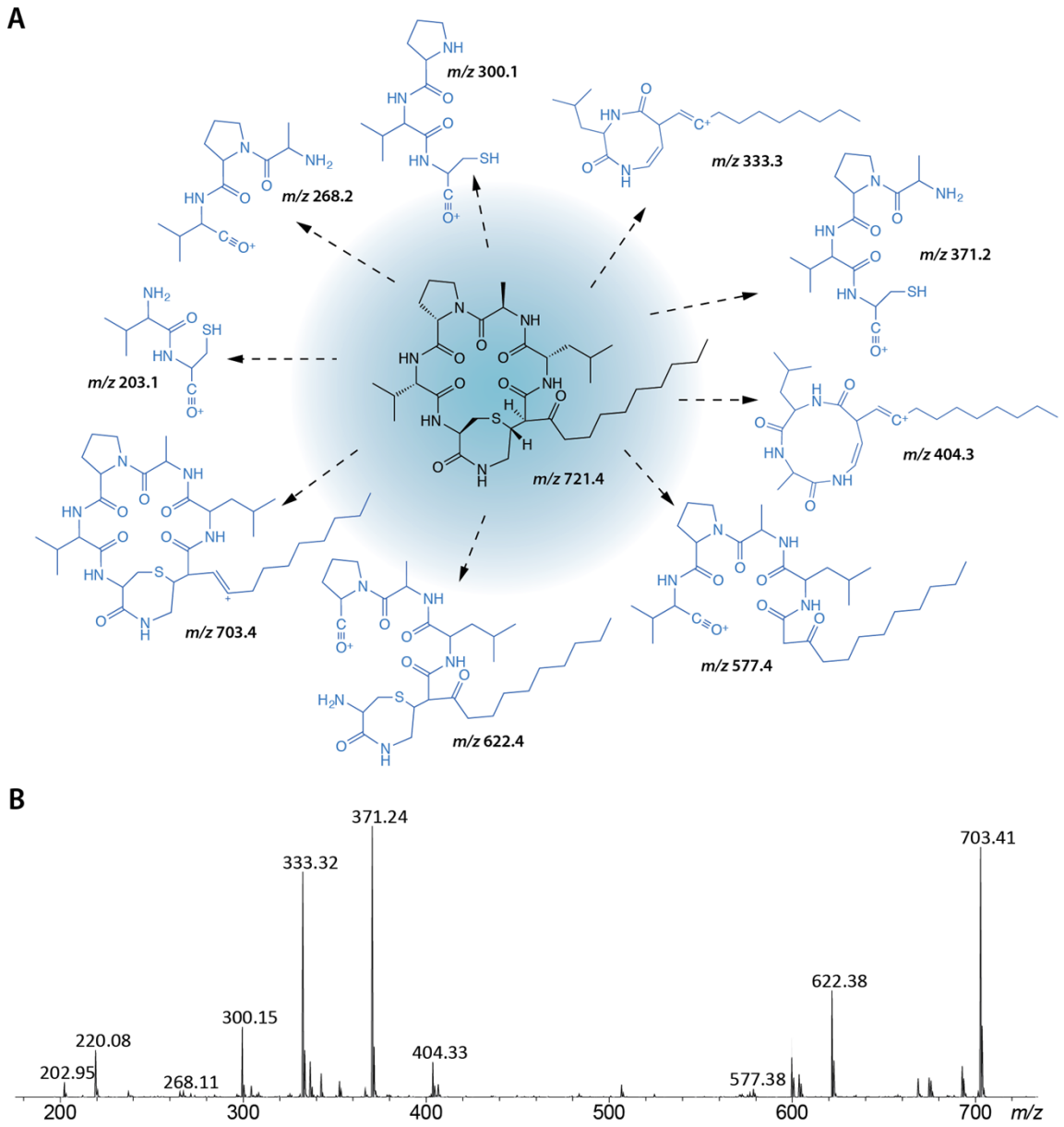

Figure S1. Fragmentation profile of mutanobactin A. **A** – fragments generated by CID have been identified and validated by incorporation of isotopically labeled amino acids and acetate. **B** – the actual MS/MS spectrum of mutanobactin A.

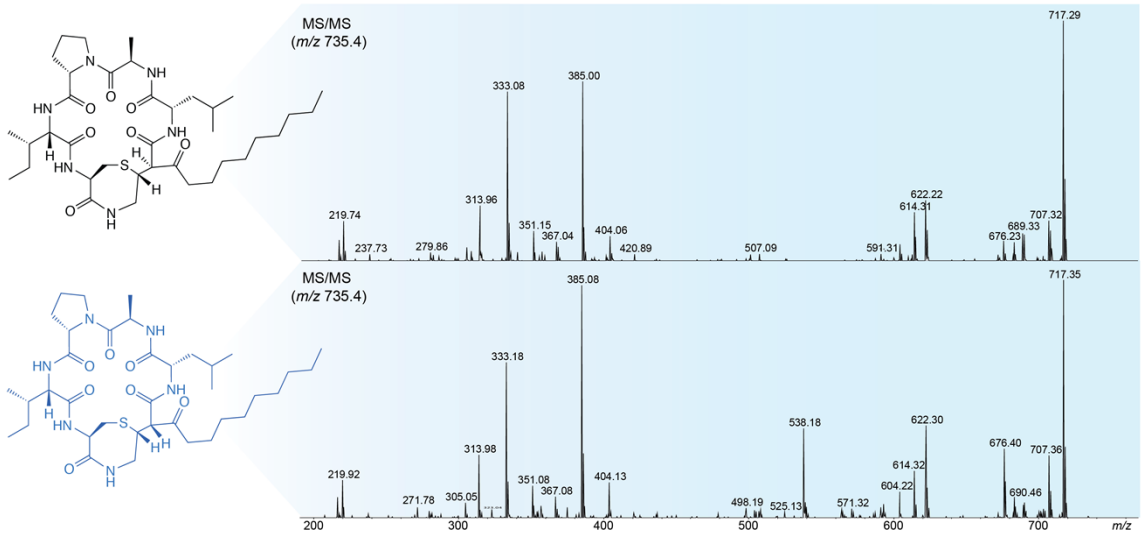

Figure S2. The fragmentation profiles of mutanobactin B and its proposed isomer. The two compounds have distinct retention times (25.7 and 30.5 min), but identical MS/MS profiles. The structure indicated in blue is the structure of the proposed isomer of mutanobactin B (mutanobactin B2). The elemental composition of mutanobactin B2 was validated using HRMS (*m/z* 735.44735 calculated, *m/z* 735.44929 observed, 2.6 ppm).

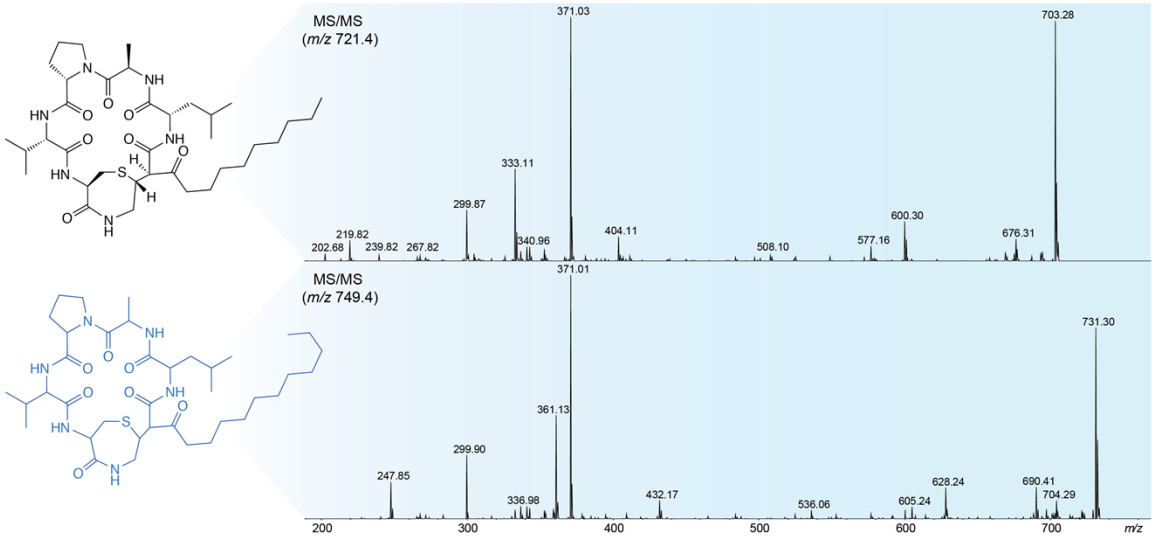

Figure S3. The fragmentation profiles of mutanobactin A and mutanobactin E. The structure of mutanobactin E (in blue) was elucidated using the combination of MS/MS and incorporation of isotopically labeled building blocks. The elemental composition of the proposed structure was validated using HRMS (*m/z* 749.46300 calculated, *m/z* 749.46314 observed, 0.2 ppm).

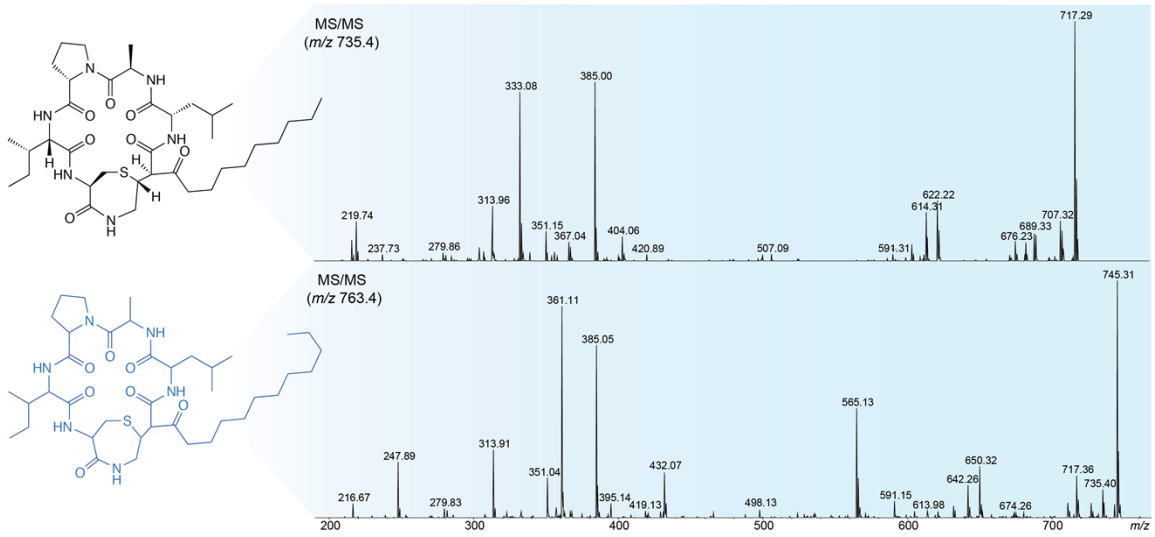

Figure S4. The fragmentation profiles of mutanobactin B and mutanobactin F. The structure of mutanobactin F (in blue) was elucidated using the combination of MS/MS and incorporation of isotopically labeled building blocks. The elemental composition of the proposed structure was validated using HRMS (*m/z* 763.47865 calculated, *m/z* 763.47872 observed, 0.1 ppm).

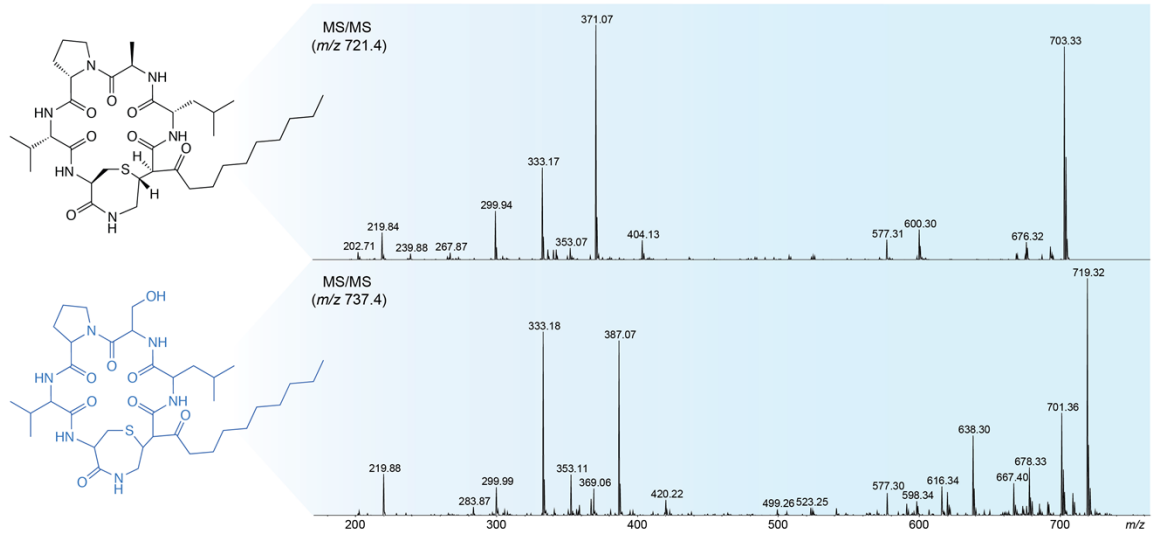

Figure S5. The fragmentation profiles of mutanobactin A and mutanobactin G. The structure of mutanobactin G (in blue) was elucidated using the combination of MS/MS and incorporation of isotopically labeled building blocks. The elemental composition of the proposed structure was validated using HRMS (*m/z* 737.4266 calculated, *m/z* 737.4280 observed, 1.9 ppm).

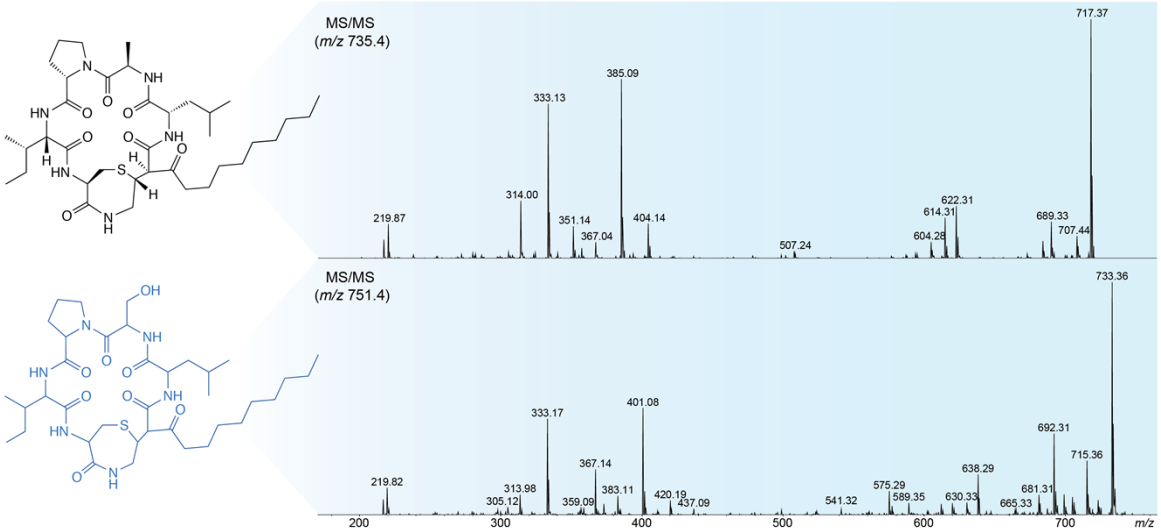

Figure S6. The fragmentation profiles of mutanobactin A and mutanobactin H. The structure of mutanobactin H (in blue) was elucidated using the combination of MS/MS and incorporation of isotopically labeled building blocks. The elemental composition of the proposed structure was validated using HRMS (*m/z* 751.44226 calculated, *m/z* 751.44384 observed, 2.1 ppm).

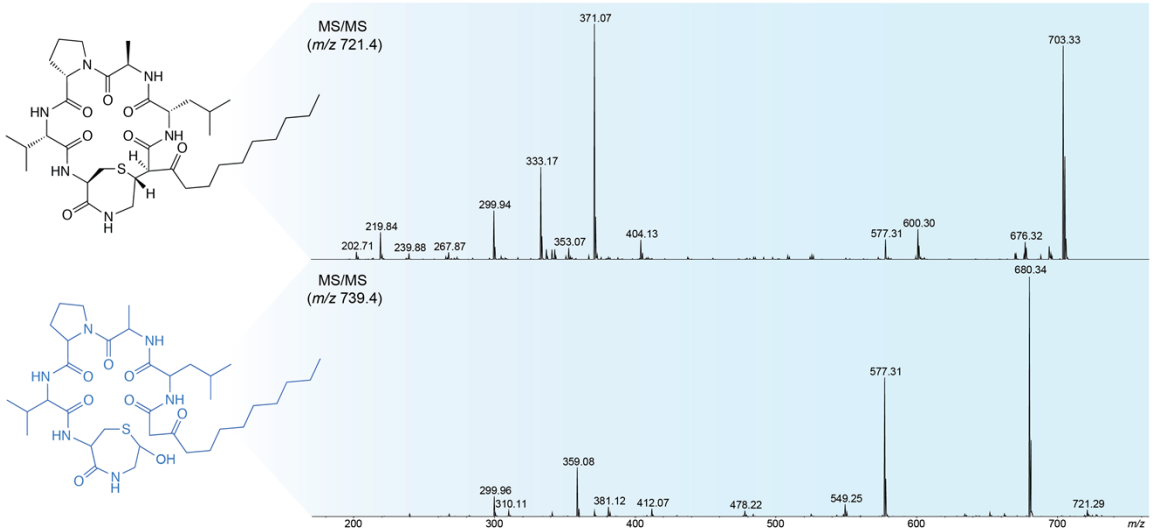

Figure S7. The fragmentation profiles of mutanobactin A and mutanobactin I. The structure of mutanobactin I (in blue) was elucidated using the combination of MS/MS and incorporation of isotopically labeled building blocks. The elemental composition of the proposed structure was validated using HRMS (*m/z* 739.44226 calculated, *m/z* 739.44243 observed, 0.2 ppm).

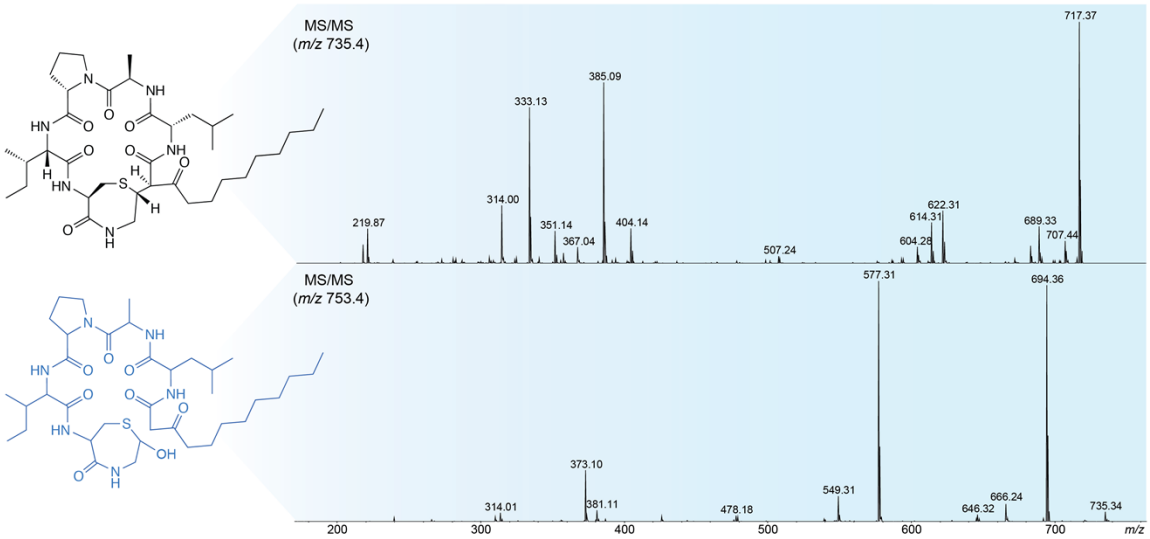

Figure S8. The fragmentation profiles of mutanobactin A and mutanobactin J. The structure of mutanobactin J (in blue) was elucidated using the combination of MS/MS and incorporation of isotopically labeled building blocks. The elemental composition of the proposed structure was validated using HRMS (*m/z* 753.45791 calculated, *m/z* 753.45800 observed, 0.1 ppm).

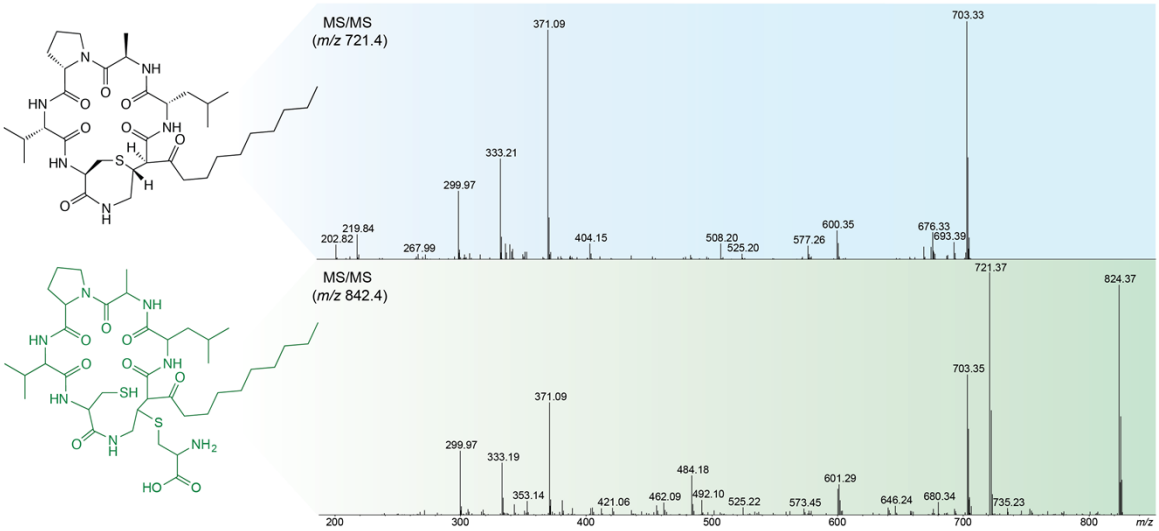

Figure S9. The fragmentation profiles of mutanobactin A and mutanolin A. The structure of mutanolin A (in green) was elucidated using the combination of MS/MS and incorporation of isotopically labeled building blocks. The elemental composition of the proposed structure was validated using HRMS (*m/z* 842.4514 calculated, *m/z* 842.4511 observed, 0.4 ppm).

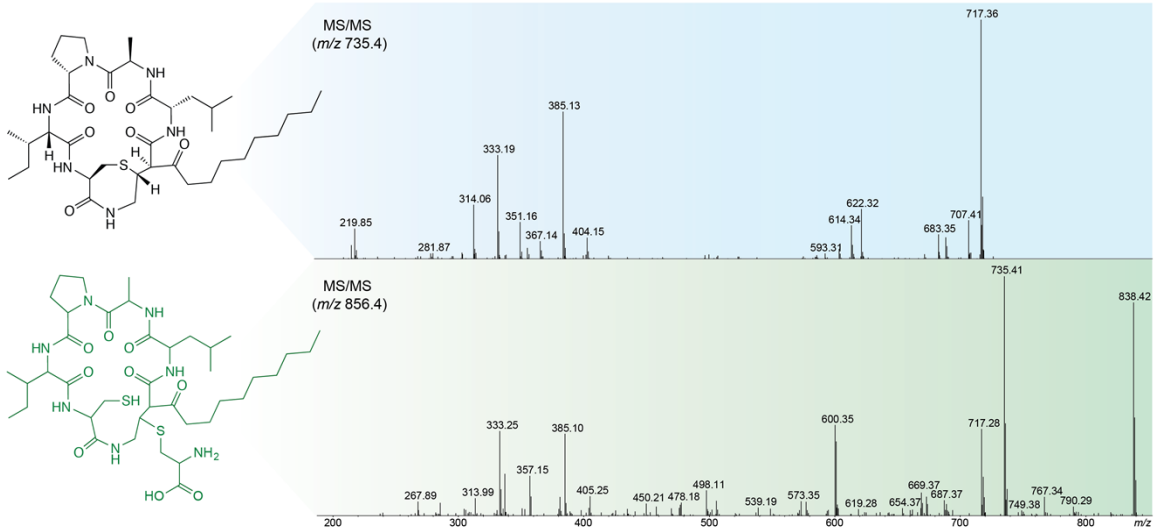

Figure S10. The fragmentation profiles of mutanobactin B and mutanolin B. The structure of mutanolin B (in green) was elucidated using the combination of MS/MS and incorporation of isotopically labeled building blocks. The elemental composition of the proposed structure was validated using HRMS (*m/z* 856.4671 calculated, *m/z* 856.4670 observed, 0.1 ppm).

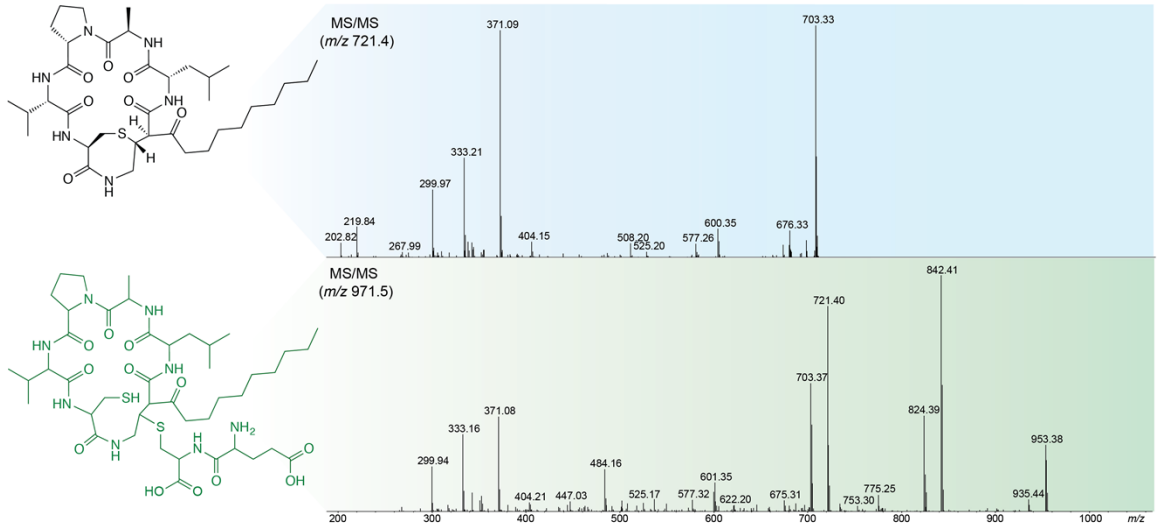

Figure S11. The fragmentation profiles of mutanobactin A and mutanolin C. The structure of mutanolin C (in green) was elucidated using the combination of MS/MS and incorporation of isotopically labeled building blocks. The elemental composition of the proposed structure was validated using HRMS (*m/z* 971.4940 calculated, *m/z* 971.4945 observed, 0.5 ppm).

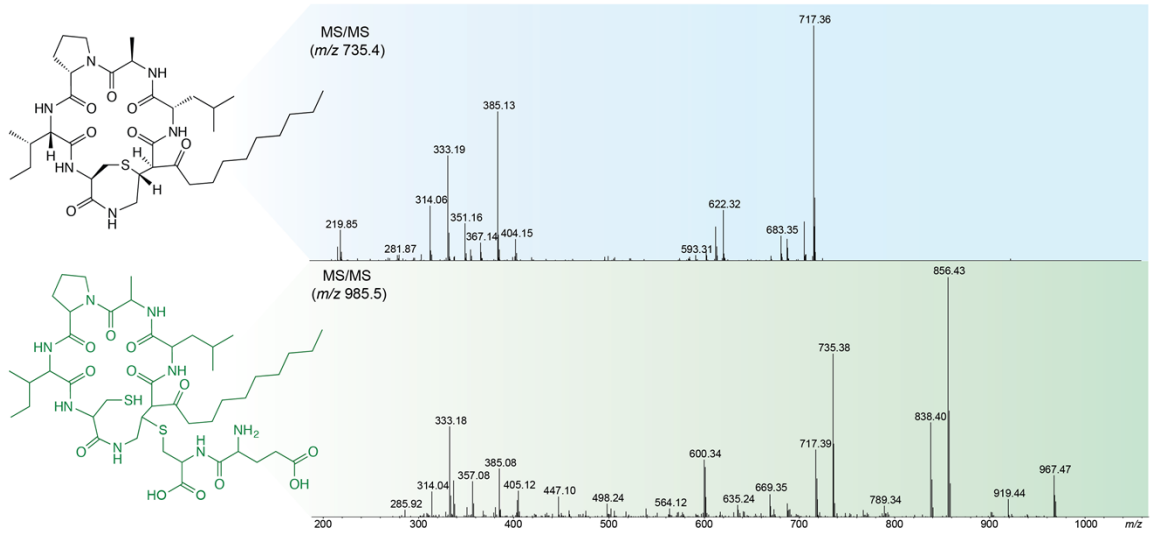

Figure S12. The fragmentation profiles of mutanobactin B and mutanolin D. The structure of mutanolin D (in green) was elucidated using the combination of MS/MS and incorporation of isotopically labeled building blocks. The elemental composition of the proposed structure was validated using HRMS (*m/z* 985.50969 calculated, *m/z* 985.50951 observed, 0.2 ppm).

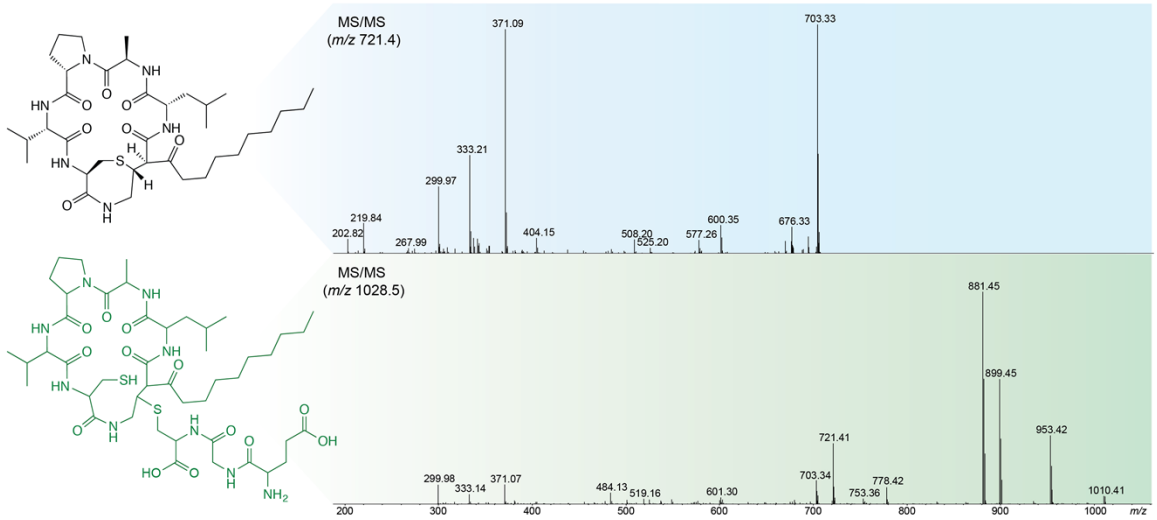

Figure S13. The fragmentation profiles of mutanobactin A and mutanolin E. The structure of mutanolin E (in green) was elucidated using the combination of MS/MS and incorporation of isotopically labeled building blocks. The elemental composition of the proposed structure was validated using HRMS (*m/z* 1028.51550 calculated, *m/z* 1028.51530 observed, 0.2 ppm).

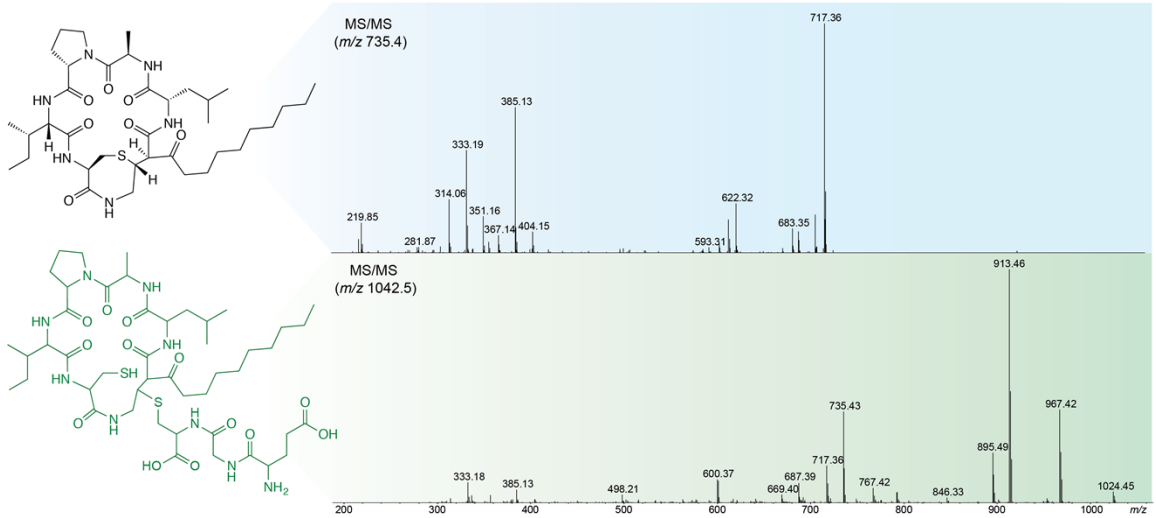

Figure S14. The fragmentation profiles of mutanobactin B and mutanolin F. The structure of mutanolin F (in green) was elucidated using the combination of MS/MS and incorporation of isotopically labeled building blocks. The elemental composition of the proposed structure was validated using HRMS (*m/z* 1042.53115 calculated, *m/z* 1042.52969 observed, 1.4 ppm).

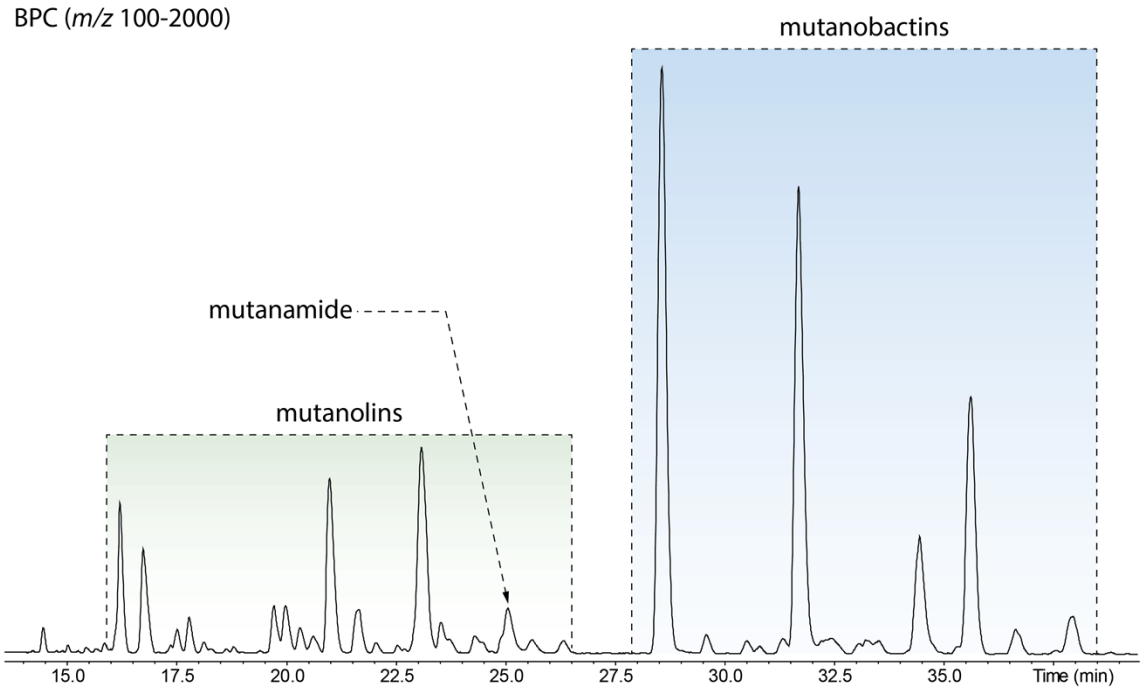

Figure S15. Base peak chromatogram of cell extract of *S. mutans* UA159. The approximate regions where mutanobactins, mutanamide and mutanolins elute are indicated.

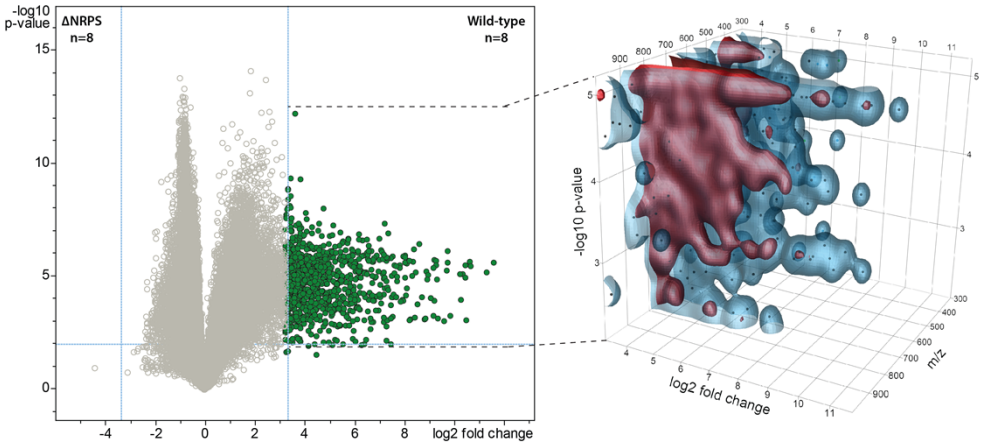

Figure S16. Clustering of metabolite features from the volcano plot. When *m/z* dimension is added to the volcano plot, molecular features pertaining to the wild-type strain (green circles) separate based on their corresponding *m/z* values. Clustering of the molecular features is represented by the contour plot, where red indicates dense clustering; two major clusters can be identified – around *m/z* 730 and *m/z* 400.

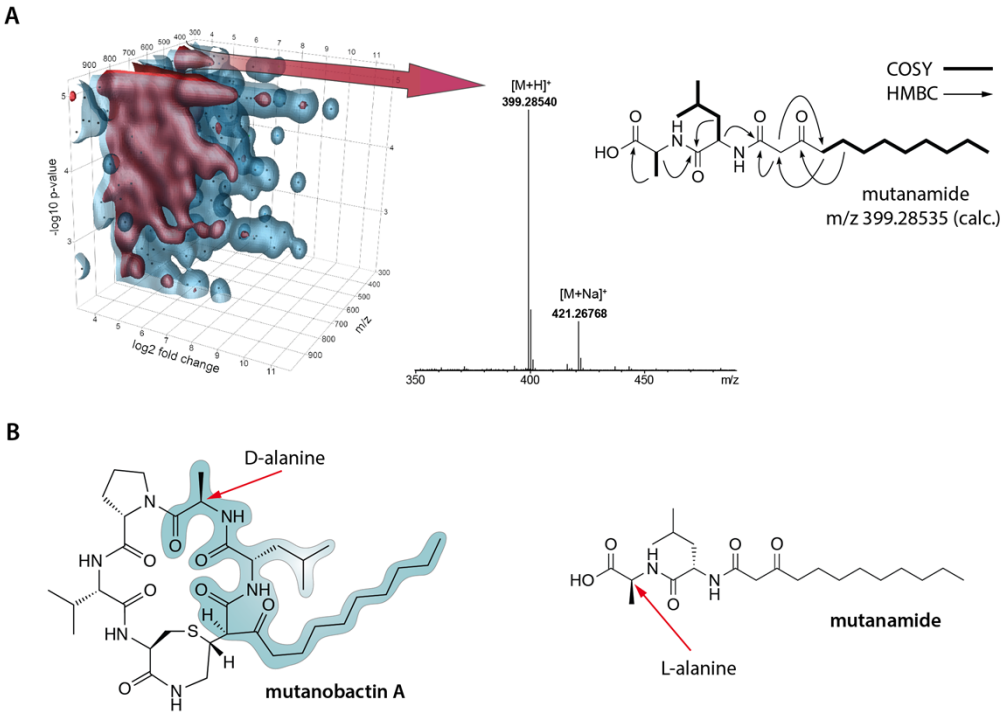

Figure S17. Identification and structure determination of mutanamide. **A** - the unexpected clustering around *m/z* 400 was due to *m/z* 399.3 (mutanamide), which was isolated and whose structure was elucidated. **B** – the chemical structure of mutanamide strongly resembles mutanobactin A, however, the latter contains D-alanine, whereas mutanamide – L-alanine.

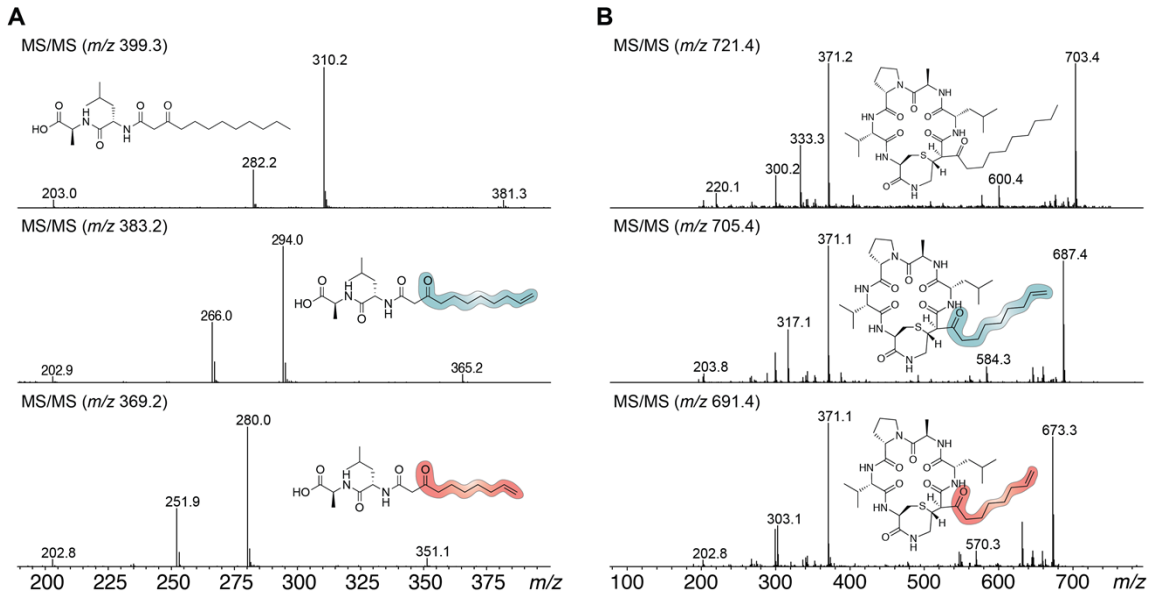

Figure S18. Fatty acid incorporation by mutanamide and mutanobactin A. **A** – MS/MS analysis of original mutanamide (*m/z* 399.3) and two analogs (*m/z* 383.2 and *m/z* 369.2) that incorporated 8-nonenoic and 7-octenoic fatty acids, respectively. **B** – MS/MS analysis of original mutanobactin (*m/z* 721.4) and two analogs (*m/z* 705.4 and *m/z* 691.4) that incorporated 8-nonenoic and 7-octenoic fatty acids, respectively.

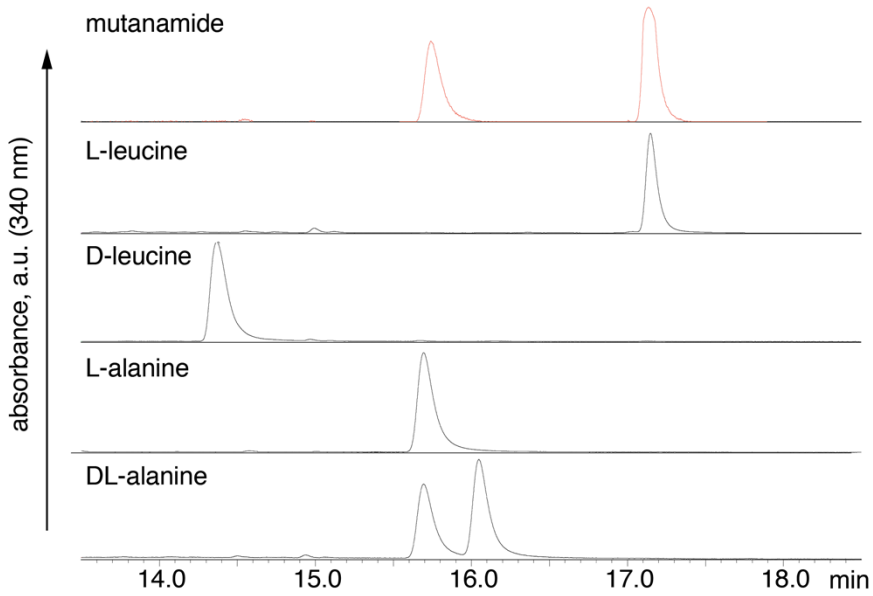

Figure S19. Results of Marfey's reaction to determine the exact stereochemistry of mutanamide. Mutanamide was fully hydrolyzed, reacted with Marfey's reagent and run on the HPLC-UV together with the L-leucine, D-leucine, L-alanine and DL-alanine standards.

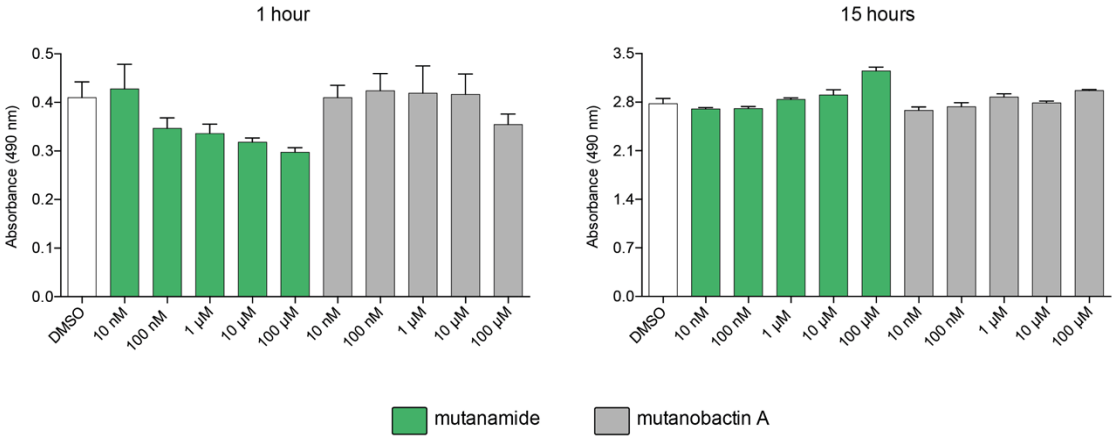

Figure S20. Antiproliferative activity of mutanamide and mutanobactin A in HT-29 cells. Both mutanamide and mutanobactin A did not have any significant effect on the growth of HT-29 cells after 1 or 15 hours.

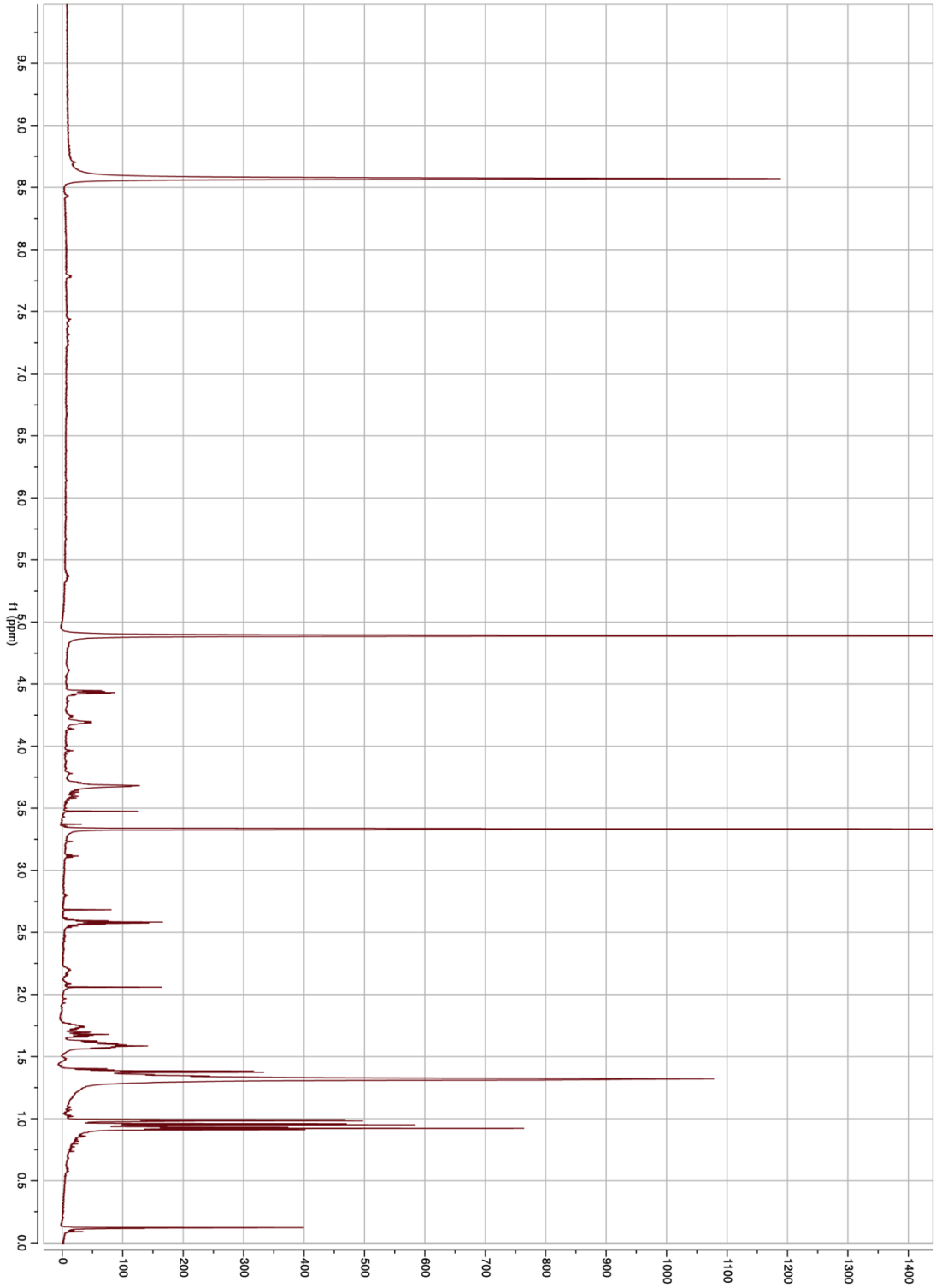

Figure S21. ^{1}H NMR spectrum of mutanamide in 100% methanol-d_4.

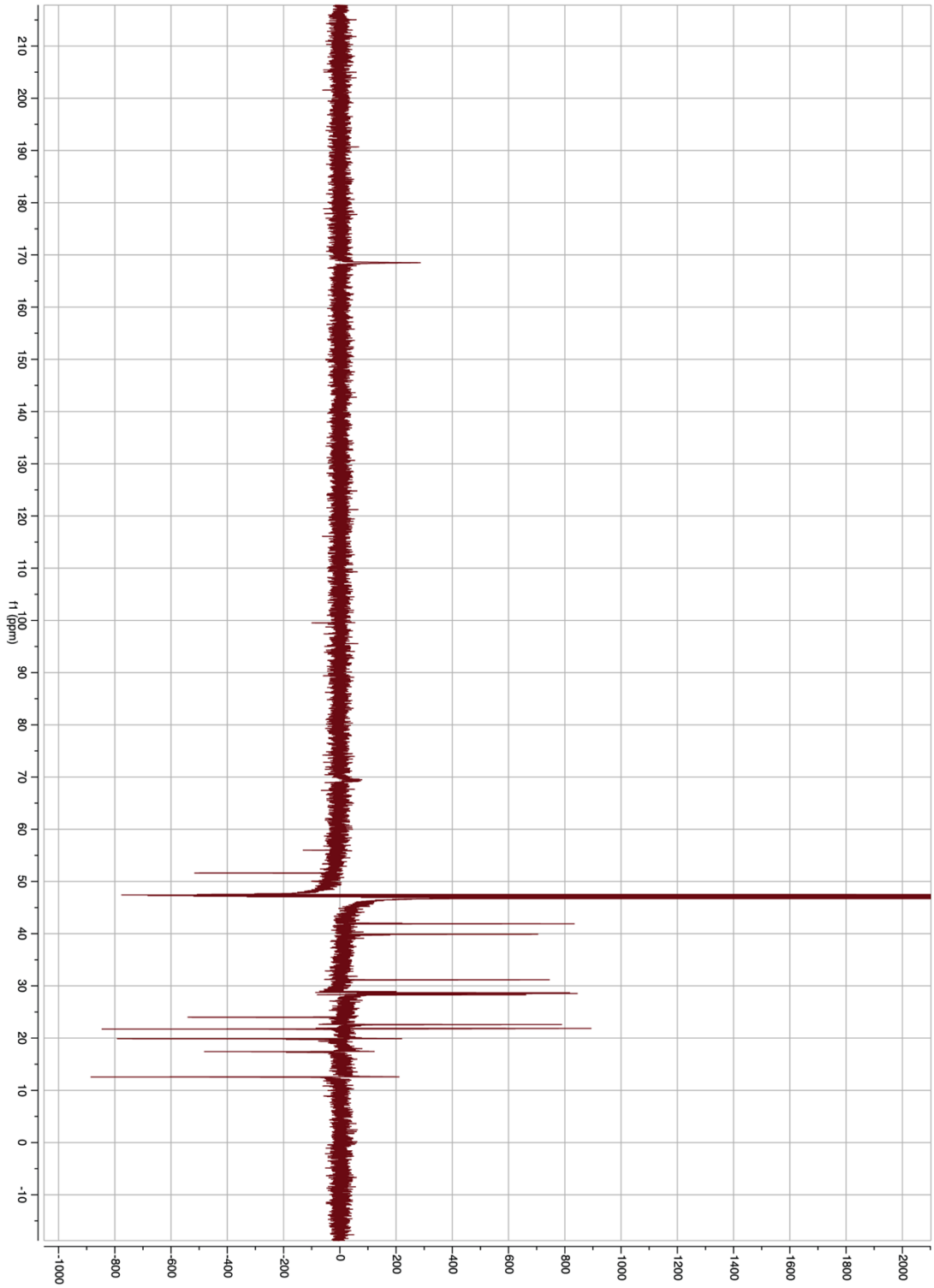

Figure S22. ^{13}C DEPTq135 NMR spectrum of mutanamide in 100% methanol-d_4.

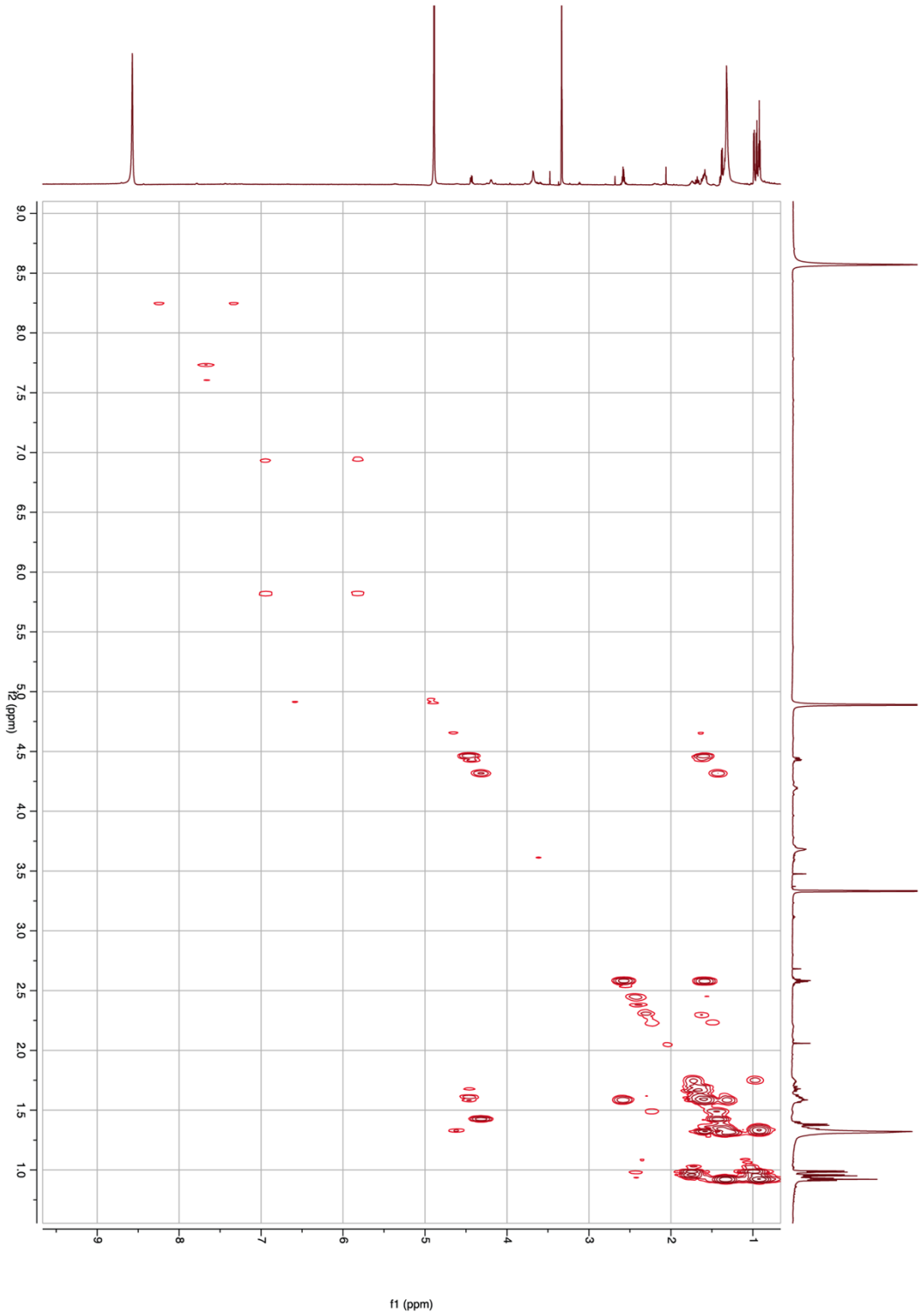

Figure S23. 2D COSY spectrum of mutanamide in 100% methanol-d_4.

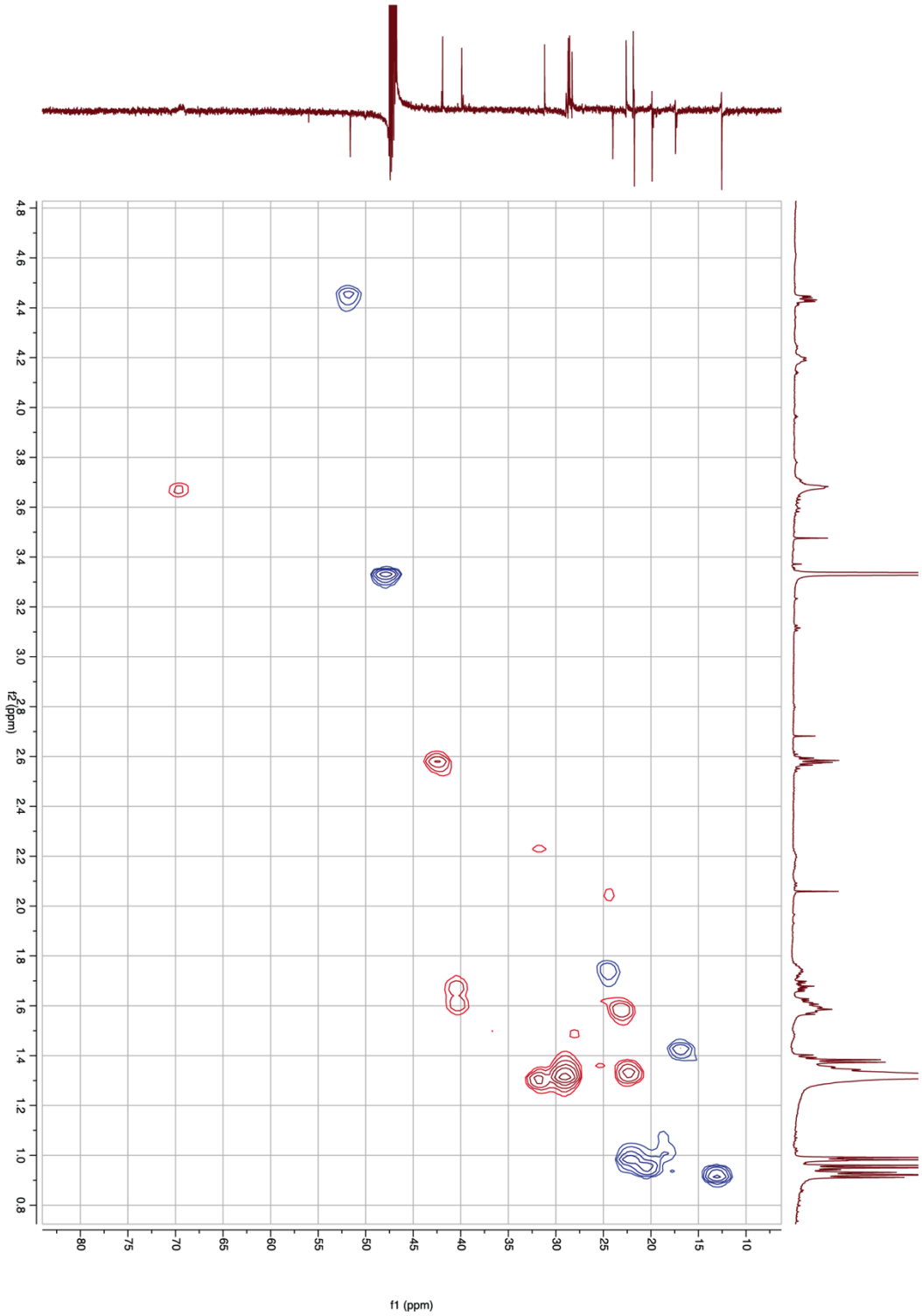

Figure S24. 2D HSQC spectrum of mutanamide in 100% methanol-d_4.

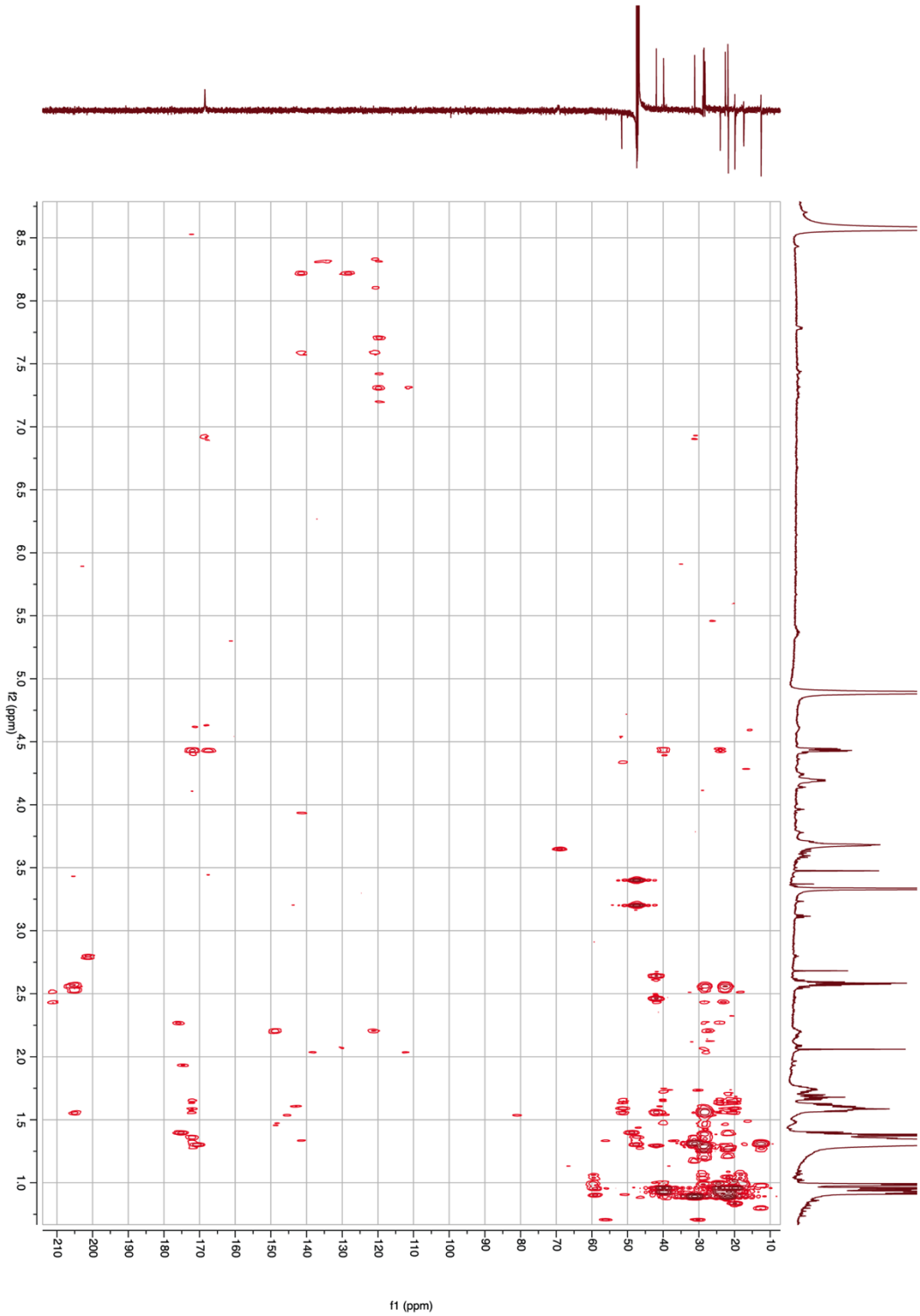

Figure S25. 2D HMBC spectrum of mutanamide in 100% methanol-d_4.

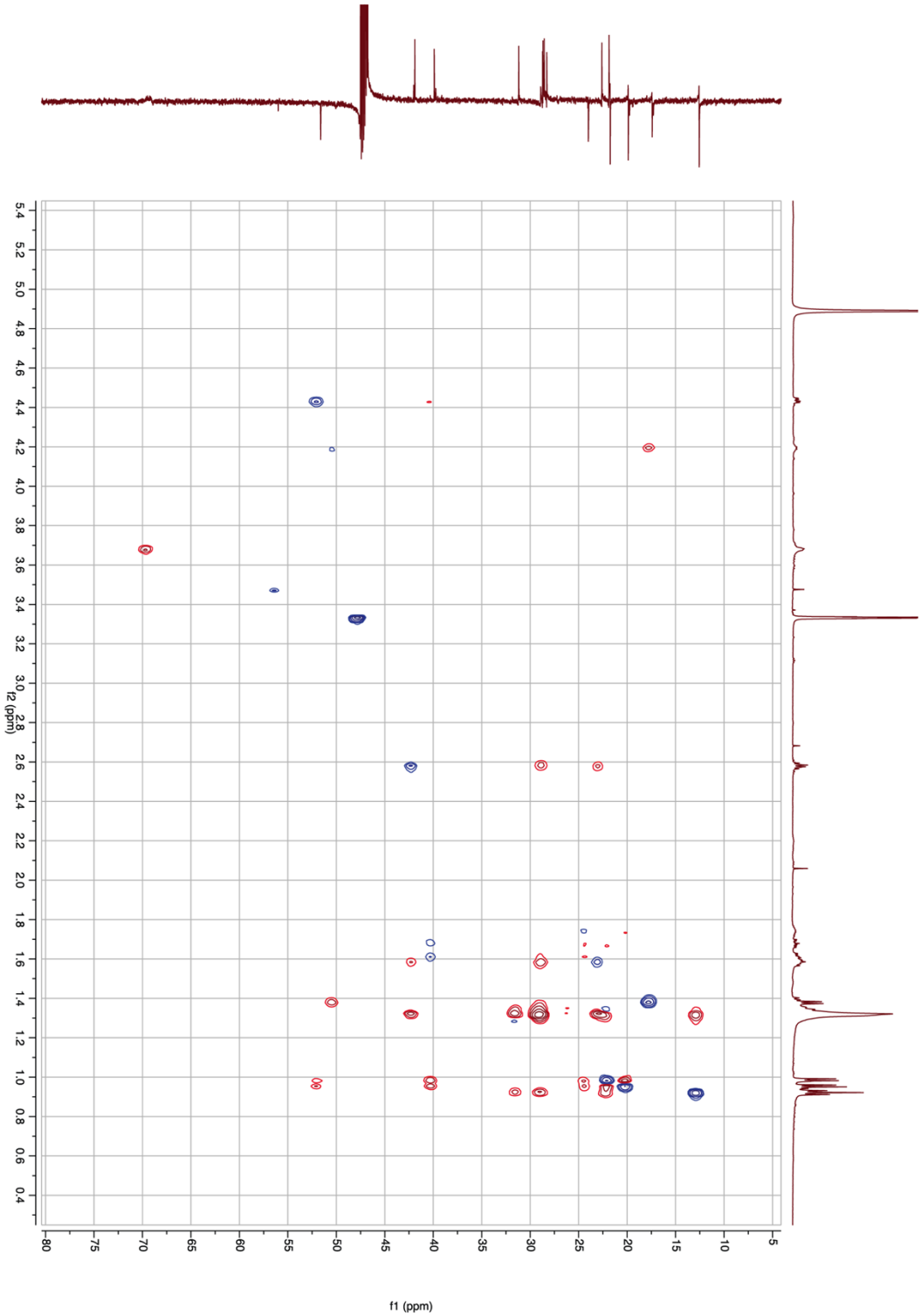

Figure S26. 2D HSQC-TOCSY spectrum of mutanamide in 100% methanol-d_4.

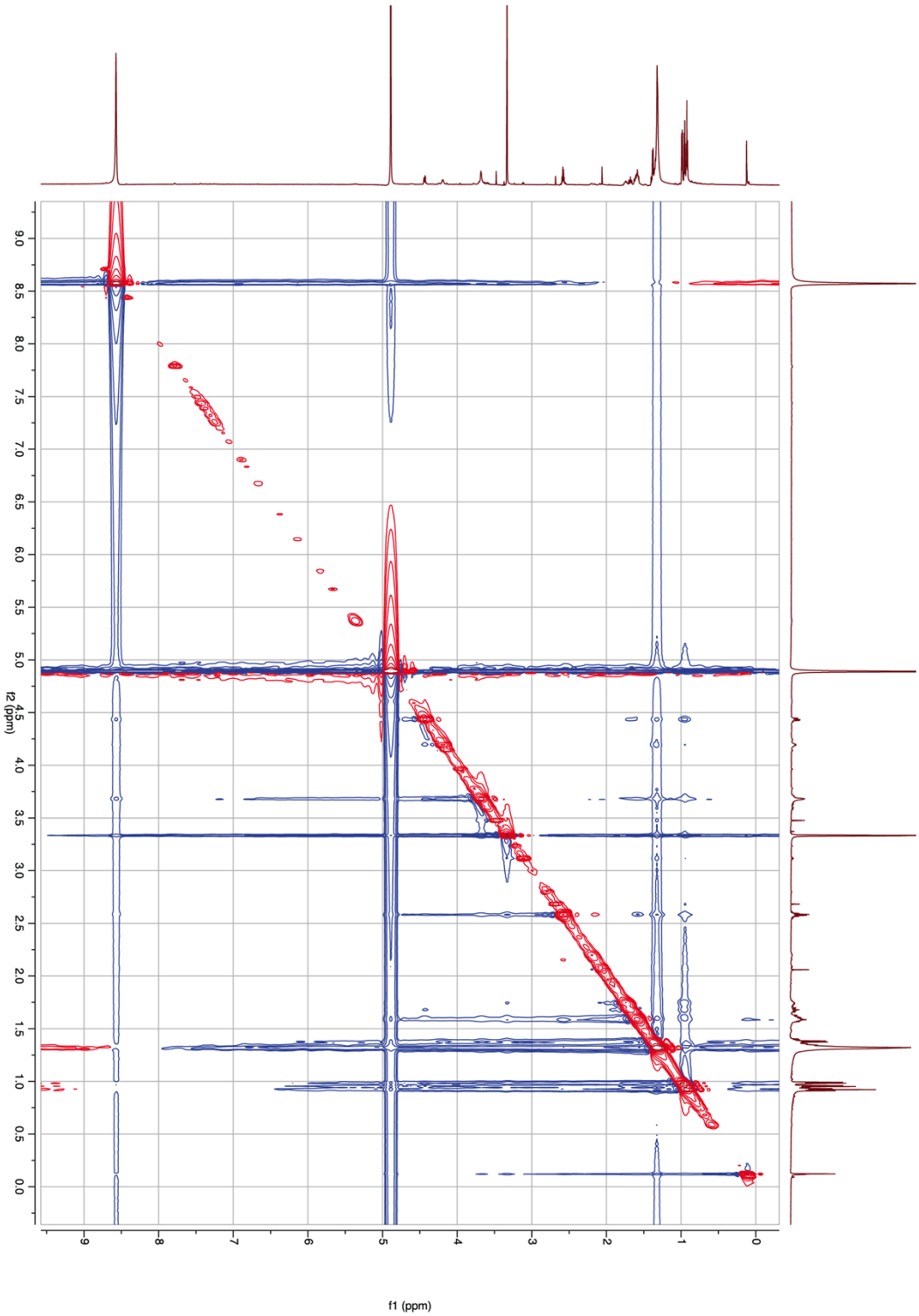

Figure S27. 2D NOESY spectrum of mutanamide in 100% methanol-d_4.